Archives of Biochemistry and Biophysics 596 (2016) 51–62

Contents lists available at ScienceDirect

Archives of Biochemistry and Biophysics

journal homepage: www.elsevier.com/locate/yabbi

Structure of the thermophilic L-Arabinose isomerase from *Geobacillus kaustophilus* reveals metal-mediated intersubunit interactions for activity and thermostability

Jin Myung Choi [a, 1], Yong-Jik Lee [b, 1], Thinh-Phat Cao [a], Sun-Mi Shin [b], Min-Kyu Park [b], Han-Seung Lee [c], Eric di Luccio [d], Seong-Bo Kim [e], Sang-Jae Lee [c], Sang Jun Lee [f], Sung Haeng Lee [a, **], Dong-Woo Lee [b, *]

[a] Department of Cellular and Molecular Medicine, Chosun University School of Medicine, Gwangju, 61452, South Korea
[b] School of Applied Biosciences, Kyungpook National University, Daegu, 41566, South Korea
[c] Major in Food Biotechnology, Silla University, Busan, 46958, South Korea
[d] School of Life Sciences, Kyungpook National University, Daegu, 41566, South Korea
[e] CJ CheilJedang, Life Ingredient & Material Research Institute, Suwon, 16495, South Korea
[f] Microbiomics & Immunity Research Center, Korea Research Institute of Bioscience and Biotechnology, Daejeon, 34141, South Korea

ARTICLE INFO

Article history:
Received 9 November 2015
Received in revised form
27 February 2016
Accepted 29 February 2016
Available online 4 March 2016

Keywords:
L-arabinose isomerase
Crystal structure
Intersubunit interaction
Substrate specificity
Thermostability

ABSTRACT

Thermophilic L-arabinose isomerase (AI), which catalyzes the interconversion of L-arabinose and L-ribulose, can be used to produce D-tagatose, a sugar substitute, from D-galactose. Unlike mesophilic AIs, thermophilic AIs are highly dependent on divalent metal ions for their catalytic activity and thermostability at elevated temperatures. However, the molecular basis underlying the substrate preferences and metal requirements of multimeric AIs remains unclear. Here we report the first crystal structure of the apo and holo forms of thermophilic *Geobacillus kaustophilus* AI (GKAI) in hexamer form. The structures, including those of GKAI in complex with L-arabitol, and biochemical analyses revealed not only how the substrate-binding site of GKAI is formed through displacement of residues at the intersubunit interface when it is bound to Mn^{2+}, but also revealed the water-mediated H-bonding networks that contribute to the structural integrity of GKAI during catalysis. These observations suggest metal-mediated isomerization reactions brought about by intersubunit interactions at elevated temperatures are responsible for the distinct active site features that promote the substrate specificity and thermostability of thermophilic AIs.

1. Introduction

L-Arabinose isomerase (AI) (E.C. 5.3.1.4), encoded by the *araA* gene of the arabinose operon, catalyzes the isomerization of L-arabinose to L-ribulose in L-arabinose catabolism [1–4]. During the past decade, several AIs have been characterized and commercially utilized to produce D-tagatose, a new antidiabetic and obesity control nutraceutical [5] that has also been 'generally recognized as safe (GRAS)' as a sweetener [6–8]. Although many attempts have been made to use microbial AIs to produce D-tagatose from D-galactose derived from lactose hydrolysis [1,8,9], mesophilic AIs yield insufficient amounts of D-tagatose for commercial purposes [1,10,11]. Because the isomerization of aldose to ketose is an endothermic reaction [7,12], the biological conversion of D-galactose to D-tagatose using thermostable AIs was found to be advantageous, as shown by the feasibility of the process, the low viscosity of substrates, the high conversion yields, and the minimal microbial contamination [1,7]. Thus, thermostable enzymes, such as AIs from *Thermotoga neapolitana* [13], *Thermotoga maritima* [7], *Thermoanaerobacter mathranii* [14], and *Thermoanaerobacter*

Abbreviations: AI, L-arabinose isomerase; CD, circular dichroism; DSC, differential scanning calorimetry; EDTA, ethylenediaminetetraacetic acid; FI, L-fucose isomerase; H-bond, hydrogen bond; ICP, inductively coupled plasma; MR, molecular replacement.

* Corresponding author.
** Corresponding author.
E-mail addresses: sunglee@chosun.ac.kr (S.H. Lee), leehicam@knu.ac.kr (D.-W. Lee).

[1] These authors contributed equally to this work.

http://dx.doi.org/10.1016/j.abb.2016.02.033
0003-9861/

saccharolyticum [15] were predicted to yield higher amounts of D-tagatose than mesophilic AIs [10,16–18]. Indeed, *T. neapolitana* AI (TNAI) and *T. maritima* AI (TMAI) isomerized D-galactose to D-tagatose at 80 °C in the presence of divalent metal ions such as Co^{2+} or Mn^{2+} with yields of ≥60% [7,13,19]. Notably, such (hyper)thermophilic AIs were found to be highly dependent on metal ions for both activity and structural stability, which distinguished them from their mesophilic counterparts [20].

By contrast to mesophilic AIs, which show little activity in the isomerization of D-galactose to D-tagatose, the reason for the promiscuous substrate preferences of thermophilic AIs that exhibit unusually high activity for D-galactose remains unclear [19,21]. Mutational studies [22,23] have suggested that the metal-dependent catalysis and thermostability of hyperthermophilic AIs at elevated temperatures may be due to structurally region-specific evolution, because the amino acid sequences of thermostable AIs are highly similar (≥70%) to those of mesophilic AIs. Notably, biophysical data and electron microscopy analysis have indicated that *Escherichia coli* L-arabinose isomerase (ECAI) is composed of hexameric subunits [24,25], although its crystal structure showed it was composed of asymmetric units with a trimeric architecture [26]. Despite the observed discrepancies between studies concerning the oligomeric state, the overall scaffold of ECAI is quite similar to the hexameric crystal structure of *E. coli* L-fucose isomerase (ECFI) [26,27], based on the observation that the crystallographic two fold axis of the ECAI structure shows a homo hexamer with D3 symmetry. In light of this, structural information about thermophilic AIs is especially important for understanding the molecular basis of thermostability and substrate specificity, compared with that of its mesophilic counterparts. Using a structural genomics approach, we recently attempted to predict the substrate-binding site of a thermophilic AI, despite the lack of 3D-structure information [28]. Our bioinformatics-guided analyses suggested that residues located at the interface between the subunits of multimeric AI would be important for catalytic cavity.

Therefore, in this study, we expressed the *araA* gene from the thermophilic bacterium *Geobacillus kaustophilus* [29–31] in *E. coli*, purified the recombinant *G. kaustophilus* AI (GKAI), characterized it, and determined for the first time the three-dimensional structure of a thermophilic AI in the presence or absence of Mn^{2+} and L-arabitol. Together with site-directed mutagenesis analysis, our data provide insight into the relationship between AI structure and function, especially regarding substrate preference, metal requirements, and thermostability, as well as providing clues to the molecular evolution of sugar isomerases that led to thermal adaptation at elevated temperatures.

2. Materials and methods

2.1. Expression and purification of GKAI

Bacterial genomic DNA was isolated using genomic DNA extraction kits (Qiagen, Germany), according to the manufacturer's instructions. The *araA* gene from *G. kaustophilus* was amplified by PCR using forward and reverse primers designed to include *Nde*I and *Hind*III restriction sites for cloning into pET-15b [32]. The *araA* gene of *G. kaustophilus* was ligated into the *Nde*I and *Hin*dIII sites of pET-15b, yielding pET-15b-GKAI. The expression vector was used to transform *E. coli* BL21(DE3), and the gene encoding GKAI was over-expressed in *E. coli* BL21(DE3) by IPTG induction. The resulting recombinant DNA in the expression vector contained a 6× His-tag and a thrombin cleavage site at the N-terminus.

N-terminal hexa-histidine tagged GKAI was purified by Ni-affinity chromatography, followed by thrombin cleavage and size-exclusion chromatography [20,32]. Typically, lysate containing over-expressed GKAI was heated at 60 °C for 30 min in prior to affinity chromatography, which facilitates further purification procedures and increases protein purity. All the mutants in this study were generated by using a standard site-directed mutagenesis technique.

2.2. Enzyme assay

AI activity was assayed by measuring the increase in L-ribulose. Unless otherwise noted, the standard reaction mixture contained 50 mM MOPS (4-morpholinepropanesulfonic acid) buffer (pH 7.5 at room temperature), 0.2 mL of enzyme preparation at a suitable dilution, 0.1 M L-arabinose, and distilled water to a final volume of 1.25 mL. The mixtures were incubated at appropriate temperatures for 20 min and stopped by chilling on ice. L-Ribulose was quantified by the cysteine-sulfuric acid-carbazole method [33], and the absorbance was measured at 560 nm. One unit of isomerase activity was defined as the amount of enzyme that produces 1 μmol of product per min under the assay conditions.

2.3. Metal content analysis and circular dichroism

To verify the metal content of AIs, column-purified enzymes were rendered metal-free and then reconstituted with pure metals as described [21,22]. The divalent metal contents of the as-isolated and EDTA-treated samples were determined by high-resolution inductively coupled plasma (ICP)-mass spectrometry on a PlasmaQuad 3 instrument at the Korea Basic Science Institute, Kyungpook National University. To verify the conformational integrity of AI, circular dichroism (CD) was determined using a Jasco J-810 spectropolarimeter with a Peltier temperature-controlled cuvette holder. The CD spectra of enzyme samples in a cuvette with a 0.1 cm path length were recorded in the far-UV region (190–240 nm). Scans were collected five times at 0.1 nm intervals with a 1 nm bandwidth. Each spectrum was corrected by subtracting the spectrum of the solution containing the buffer used, with and without Mn^{2+}.

2.4. Differential scanning calorimetry (DSC) measurement

Calorimetric measurements were performed using a VP-DSC microcalorimeter (Microcal Inc. GE Healthcare, Northampton, USA). All scans were run at pH 7.4 in 1 mM potassium phosphate buffer, in a temperature range from 20 to 100 °C at a rate of 90 °C/h. The cell volume was 0.8 mL. The apo-GKAI (160 μM) incubated with 1 mM Mn^{2+} (Mn^{2+}-GKAI) for 2 h at 25 °C. The potassium phosphate buffer was used for baseline scans. The apparent T_m values of GKAI with and without metal ions were determined. Data from Microcal were analyzed using the software Origin 8.0.

2.5. Kinetics

The kinetic parameters of wild-type and mutant AIs were determined in the same reaction mixtures as described above, except that AIs were assayed over 1 min to obtain the initial reaction rates. The concentrations of L-arabinose ranged from 0 to 40 mM. Kinetic results were obtained by fitting the data with a Michaelis-Menten equation using the software Origin 8.0.

2.6. Protein crystallization and X-ray crystallography

Purified GKAI was concentrated to 6–9 mg/mL in an appropriate buffer with or without Mn^{2+} and crystallized by using a hanging-drop vapor diffusion technique. The ligand complex of GKAI was obtained by soaking Mn^{2+}-GKAI crystals in 10 mM L-arabitol. X-ray

experiments were performed at Pohang Light Source (PLS), beamline 5C and 7A (Pohang, South Korea) using an ADSC Q315r and ADSC Q270 CCD detectors, respectively, and all three structures of GKAI were determined by molecular replacement (MR) using a monomeric apo form of ECAI structure (2AJT) as a search model [26]. A subsequent refinement and model building process reduced the R_{work} and R_{free} values to the reliable ranges for all the three models (Table 1). In particular, the L-arabitol PDB file was created using the PHENIX program LIGANDFIT [34] and fitted into mF_o-DF_c density consistent with the ligand during the building of the L-arabitol -Mn^{2+}-GKAI model. Similar to ligand-bound GKAI, Mn^{2+} ion was also found in the electron density map for both of holo- and L-arabitol -Mn^{2+}-GKAI.

2.7. Accession numbers

Database: structural data are available in Protein Data Bank, www.pdb.org under the accession number 4R1O (apo-GKAI), 4R1P (holo-GKAI), and 4R1Q (holo-GKAI in complex with L-arabitol).

3. Results

3.1. Biochemical characteristics of thermophilic GKAI

The *araA* gene (1.5 kb) encoding GKAI was cloned and successfully expressed in *E. coli* BL21(DE3) as an N-terminal 6× His-tagged fusion protein with a thrombin cleavage site upon induction with IPTG as described previously [32]. GKAI was purified by heat treatment, a Ni^{2+}-chelate affinity chromatography, and thrombin treatment to remove the His-tag residues. The apparent M_r of the protein was estimated to be 56 kDa by SDS-PAGE, consistent with the value of M_r (56,236) calculated from the presumptive amino acid sequence. Subsequent size-exclusion gel chromatography showed that the molecular mass of the native protein was an estimated 336 kDa (Fig. 1A), indicating that the heterologously expressed GKAI is a homohexamer, a finding consistent with that of ECAI [25]. High-resolution ICP-mass spectrometry showed that, following purification, the recombinant GKAI contained an estimated 0.06 ± 0.001 equivalents of Mn^{2+} per subunit. Other divalent metal ions (e.g., Co^{2+}, Ca^{2+}, Cd^{2+}, Cu^{2+}, Mg^{2+}, Fe^{2+}, Ni^{2+}, and Zn^{2+}) were not detected in the purified enzyme. Further, GKAI that had been treated with EDTA and subsequently isolated by dialysis contained only trace amounts of metals, including Mn^{2+} (<0.01 ± 0.003 equivalents per monomer), indicating EDTA is an effective chelator of AI-bound metal cations.

The temperature dependence of the recombinant enzyme was determined by incubating the apo-GKAI at various temperatures for 20 min in the presence and absence of 1 mM Mn^{2+} (Fig. 1B). Under these assay conditions, GKAI exhibited maximal activity at 60 °C in the presence of 1 mM Mn^{2+}. Incubation of GKAI at 60 °C for 120 min in the presence of 1 mM Mn^{2+} caused no loss of AI activity, whereas 50% of activity was loss after incubation at 70 °C for 29.2 min (Fig. 1C). Consequently, the apo-GKAI was 1.5- to 9-fold less stable than the holo-GKAI at 60 °C and 70 °C, respectively, indicating that GKAI was thermostabilized by Mn^{2+}, a finding consistent with thermophilic AIs [7,20,21]. Purified GKAI had high activity at pH 7.5 (Fig. 1D). As shown in Fig. 1E, EDTA-treated GKAI showed significantly decreased activity (less than 25% compared with GKAI in the presence of 1 mM Mn^{2+}) in the absence of divalent metal ions. However, addition of 1 mM Mn^{2+} to the apo-GKAI restored enzymatic activity, until it was 84% that of As-isolated GKAI, consistent with the divalent metal ion requirements of other thermophilic AIs [7,14,15,19]. Other divalent metal ions were tested, including Co^{2+}, Mg^{2+}, Ca^{2+}, Fe^{2+}, Ni^{2+}, Zn^{2+}, and Cu^{2+}, with GKAI strongly activated in the presence of Mg^{2+} (117% compared with Mn^{2+}), Ca^{2+} (106%), and Co^{2+} (58%). These results indicate

Table 1
Statistics for data collection and refinement of GKAI.

	Apo-GKAI (PDB ID 4R1O)	Mn^{2+}-GKAI (4R1P)	GKAI-Mn^{2+}- L-arabitol (4R1Q)
Data collection			
Beam line	PAL-7A	PAL-5C	PAL-5C
Space group	$P2_12_12_1$	$C2$	$P2_12_12_1$
Wavelength (Å)	1.00150	0.97951	1.00001
Unit-cell parameters (Å °)	a = 116.72, b = 140.75, c = 215.82 α = β = γ = 90.00°	a = 223.66, b = 153.12, c = 91.24 α = γ = 90.00°, β = 103.85°	a = 118.51, b = 146.26, c = 215.68 α = β = γ = 90.00°
Resolution (Å)	50–2.40 (2.44–2.40)	50–2.30 (2.34–2.30)	50–2.25 (2.29–2.25)
Total reflections	982633	629574	2123676
Unique reflection	133329	131054	175982
Completeness (%)	96.2 (94.1)	99.5 (99.1)	99.2 (99.4)
Redundancy	7.4 (7.1)	4.8 (4.7)	12.1 (11.4)
R-merge[a] (%)	11.5 (45.9)	14.4 (83.3)	11.2 (45.9)
Average I/σ (I)	14.091 (3.75)	18.33 (2.81)	20.576 (5.29)
Solvent content (%)	45.41	45.31	48.23
Matthews coefficient (Å ^{3}Da^{-1})	2.25	2.25	2.37
Refinement			
R_{work}/R_{free} (%)	16.43/21.58	15.56/21.29	15.38/20.12
Protein residues	2970	2962	2972
Waters	1182	1171	1645
Mn		6	6
L-arabitol			6
RMSD			
Angle (°)	1.091	1.094	1.071
Length (Å)	0.007	0.008	0.007
Wilson B factor (Å^2)	25.6	28.3	29.8
Ramachandran plot			
Most favored regions (%)	96.48	97.19	97.37
Allowed regions (%)	3.45	2.61	2.57
outliers	0.07	0.20	0.07

Values in parentheses correspond to highest resolution shell.
[a] R-merge = $\Sigma_{hkl}\,\Sigma_i\,|I_i(hkl)-\langle I(hkl)\rangle|/\Sigma_{hkl}\,\Sigma_i\,I_i(hkl)$, where $I_i(hkl)$ is the observed intensity and $\langle I(hkl)\rangle$ is the average intensity of symmetry-related observations.

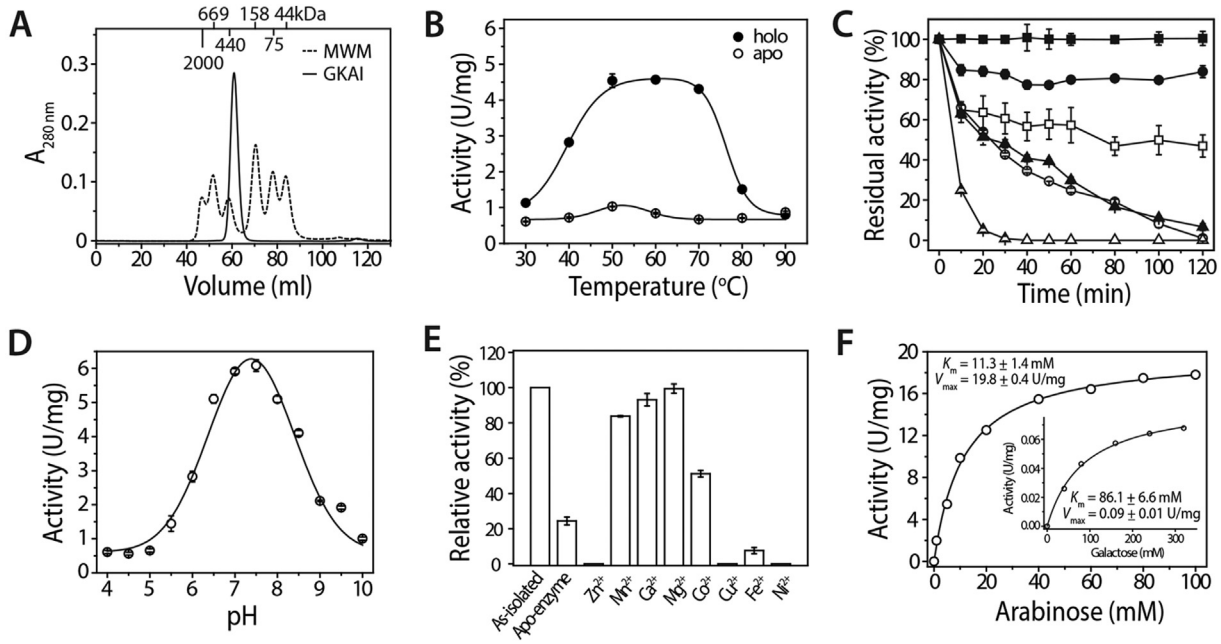

Fig. 1. Biochemical and biophysical characterization of GKAI. (A) Size-exclusion chromatography of recombinant GKAI. A superdex 200 16/60 column was run at a flow rate of 1.0 mL/min, and the elution profile was monitored at 280 nm. The column was calibrated with blue dextran (2000 kDa), thyroglobulin (669 kDa), ferritin (440 kDa), aldolase (158 kDa), conalbumin (75 kDa), and ovalbumin (44 kDa) as standards. (B) Effect of temperature on recombinant GKAI activity. The temperature dependence of recombinant GKAI was determined by incubating the apo and holo enzymes at various temperature (30–90 °C) for 20 min. (C) Time course of irreversible thermal inactivation of purified GKAI. After various incubation at 60 °C (square), 65 °C (circle), and 70 °C (triangle) in the absence of Mn^{2+} or in the presence of 1 mM Mn^{2+}, aliquots were withdrawn, and their residual activities were measured under the standard conditions. Open and closed symbols represent data points for the apo and holo enzymes, respectively. (D) Effect of pH on recombinant GKAI activity. The pH dependence of recombinant GKAI was determined by cysteine-sulfuric acid-carbazole method to calculate the product after 20 min incubation at various pH values. (E) Effect of divalent metal ions on GKAI activities. Reaction mixtures contained GKAI as metal-free enzymes (0.1 mg/ml) in the presence of 1 mM each metal ions. Activity was measured at 60 °C in triplicate under standard assay conditions without addition of 1 mM Mn^{2+}. (F) The rates for GKAI-catalyzed isomerization at various concentrations of L-arabinose as the substrate.

that the catalytic activity of GKAI is strongly dependent on divalent metal ions, a finding previously reported for thermophilic AIs [7,20,21]. Kinetic parameters were determined by steady-state kinetic analyses with L-arabinose and D-galactose as substrates. GKAI reactions yielded typical Michaelis-Menten curves, with the steady-state kinetic values of K_m, V_{max}, k_{cat}, and k_{cat}/K_m for L-arabinose and D-galactose as substrates (Fig. 1F). Although the k_{cat}/K_m value of GKAI is much greater for L-arabinose than for D-galactose, the enzyme showed higher activity in converting D-galactose to D-tagatose than other mesophilic counterparts [1,10,11,20].

3.2. Overall architecture of GKAI

The crystal structures of the apo form of thermophilic GKAI and of its holo form with and without L-arabitol as a substrate analogue were determined at resolutions of 2.40 Å, 2.30 Å and 2.25 Å, respectively. In these structures, most amino acids, as well as metal ions and substrates, were well fitted to their respective electron density maps with reliable statistics (Table 1). All the solved structures contained six subunits (M1, M2, M3, M4, M5, and M6), which formed a sandwich-like homo-hexamer found in an asymmetric unit with two main non-crystallographic symmetries: the 3-fold symmetry in the homo-trimer and the 2-fold symmetry between the two trimers (Fig. 2A and B). The subunits of the hexameric structures of apo-GKAI, Mn^{2+}-GKAI, and Mn^{2+}-GKAI bound to L-arabitol were found to be superimposable, with C^{α} r.m.s. deviations of 0.27–0.62 Å, 0.20–0.30 Å, and 0.18–0.25 Å, respectively. Although the crystal packing of mesophilic ECAI contains a trimer in the asymmetric unit [26], our size-exclusion chromatography results (Fig. 1A), together with structural and biochemical data, strongly suggested that GKAI may consist of a hexamer composed of six identical subunits.

A ribbon representation of the overall monomer structure of GKAI is shown in Fig. 2C. The root mean square deviations for C^{α} atoms and Z-scores of DALI search [35] for monomeric apo-GKAI were 0.76 Å and 51.9, respectively, with monomeric apo-ECAI (PDB code 2AJT, 60% identity), and 2.9 Å and 31.8, respectively, with apo-ECFI (1FUI, 11% identity), suggesting that the overall scaffold of GKAI is quite similar to those of sugar isomerases such as ECAI and ECFI (Fig. 2D and E). Indeed, each monomeric subunit of GKAI can be divided into three domains: the N-terminal domain (N terminus-Leu177), the central domain (Lys178-Gly325), and the C-terminal domain (Lys326-end), with each subunit composed of 17 α-helices and 18 β-strands (Fig. 2C). A typical Rossmann fold, structurally similar to nucleotide binding domain, is found in the N-terminal domain, where five parallel β-strands (β1- β5) alternative with five α-helices (α1–α3 and α5–α6). Although the organization of overall secondary structural elements in the central domain is similar to that of the N-terminal domain, it only contains four parallel β-strands (β6–β9), with links within helices (α6–α13) not appearing to be Rossmann folds. The C-terminal domain contains an antiparallel β-barrel composed of six β-strands (β10–β11 and β14–β17). The three designated domains of each monomeric GKAI forms interfaces with two other monomers, allowing them to cooperatively participate in the formation of active sites in functional homo-hexamers (see below for details).

3.3. The metal-binding site of GKAI

The initial active sites of GKAI structures have been proposed as corresponding to the putative active site of apo-ECAI [26]. As shown in Fig. 3A, the cavity between the N-terminal domain of one

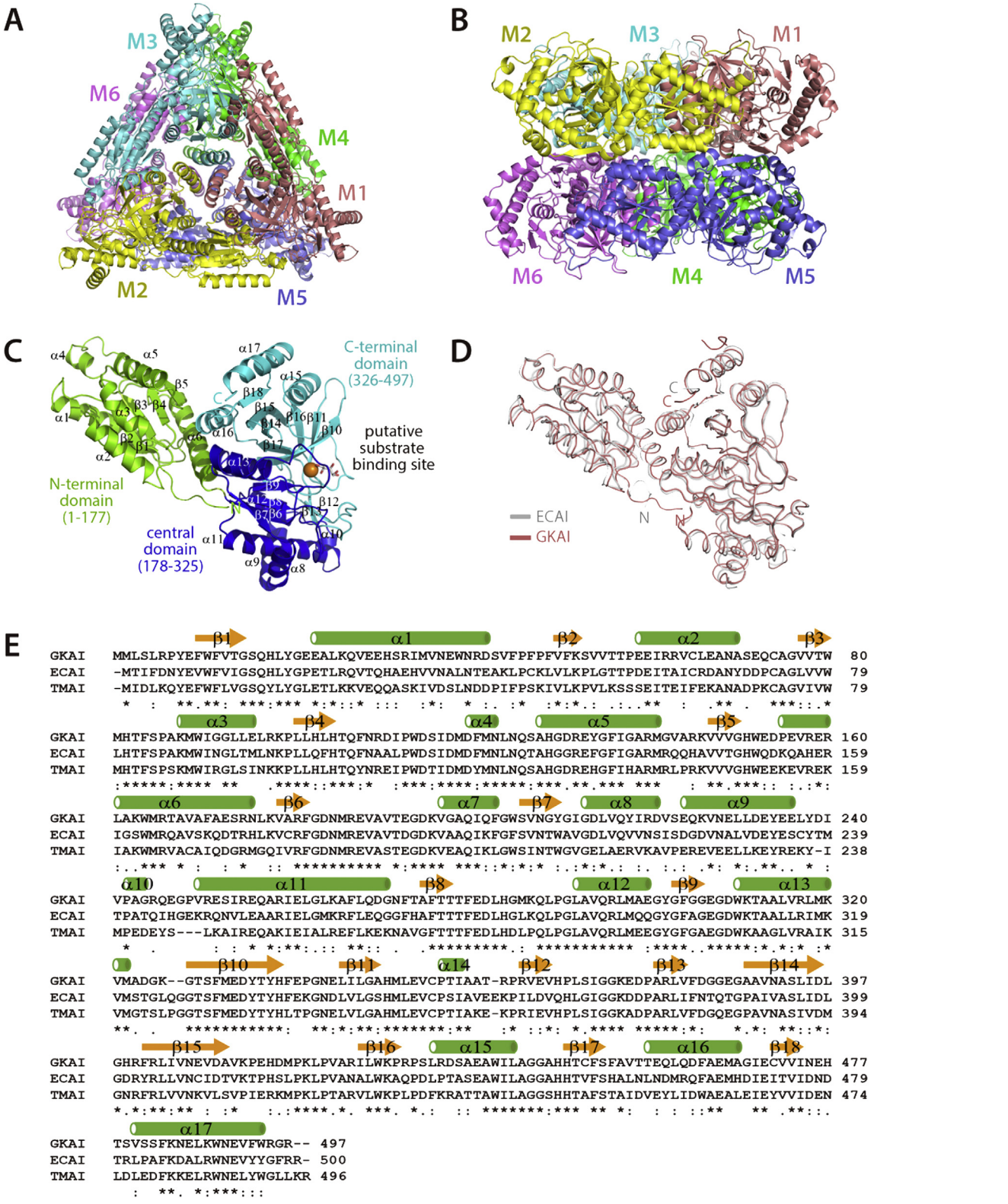

Fig. 2. Overall structure of GKAI. Top view (A) and side view (B) of the hexamer structure. The six molecules are colored in salmon (M1), yellow (M2), aquamarine (M3), green (M4), slate (M5), and violet (M6). (C) Ribbon representation of detailed subunit structure of GKAI in complex with Mn^{2+}. The structure of GKAI is comprised of the N-terminal domain shown in green, the central domain in cyan, and the C-terminal domain in blue. The small orange sphere indicates metal ion. (D) Superimposed structure of monomer of apo-GKAI (4R1O) with that of apo-ECAI (2AJT). Each monomer is colored in deep salmon and white, respectively. (E) Alignment of the amino acid sequences of AIs from *G. kaustophilus*, *E. coli*, and *T. maritima*. Secondary structure elements are shown with cylinders (α-helices) and arrows (β-strands) above the sequence. (For interpretation of the references to colour in this figure legend, the reader is referred to the web version of this article.)

subunit, consisting of the α-helices (α4, α5), β1–α1 loop, and the β3–α3 loop from one subunit (M1 subunit) and loops in the central and C-terminal domains from the neighboring subunit (M2), is like a substrate-binding site. Notably, the neighboring subunit seems to provide the metal and substrate-binding residues on β6–α7, β9–α13 and α15–β17. The active sites of both holo-GKAI and L-arabitol bound GKAI around six inter-subunit clefts exhibit Mn^{2+} ions, with strong differences between electron density maps followed by subsequent refinement. Since we added Mn^{2+} to apo-GKAI in screening crystals, the metal ions bound to GKAI were assumed to be Mn^{2+}. Moreover, the ICP spectrum of an as-isolated form also showed the presence of Mn^{2+}. The bound metal ions are located at the cleft region of each subunit and coordinated in a distorted tetrahedral form with Glu307, Glu332, His349, and His448 (Fig. 3B). The distance between Mn^{2+} and the N^{ε} atoms of His349 and His448 were 2.54 Å and 2.45 Å, respectively, and the distance between Mn^{2+} and the $O^{\delta 2}$ atoms of Glu307 and Glu332 were 2.43 Å and 2.47 Å, respectively. As shown in Fig. 4 and Table 2, circular dichroism (CD) data demonstrated that site-directed mutagenesis on the four residues involved in metal binding did not affect the secondary structures of individual single mutant AIs except H448A. Nevertheless, these mutants exhibited very little activity and/or low catalytic efficiencies (k_{cat}/K_m) even in the presence of Mn^{2+}. Thus these results clearly demonstrated that the metal-binding site of GKAI consisted of the four residues above. As shown in Fig. 3A, six water molecules at the active site of apo-GKAI were apparently H-bonded to hydrophilic residues, including Glu307, His447, and Glu332. In holo-GKAI, Mn^{2+} appeared to replace the water molecules coordinated by four residues (Glu307, Glu332, His349, and His448) (Fig. 3A). Upon the entry of the substrate analogue L-arabitol into the active site, additional two water molecules are pushed out and three residual water molecules appeared to stabilize the substrate by forming strong H-bond networks, together with Mn^{2+} (Fig. 3A).

3.4. The substrate-binding site of GKAI

The difference Fourier maps (mF_o-DF_c) revealed a strong electron density for bound L-arabitol as the substrate analogue deep in the intersubunit cleft formed among the three domains and with coordination distances of atoms in the enzyme-substrate complexes (Fig. 3). Each active site bound to L-arabitol was located in a cleft between the C-terminal domain and the central domains of the subunit adjacent to the other subunit interface (i.e., the N-terminal domain) (Fig. 3B). The O1 atom of L-arabitol coordinates with Mn^{2+}, Glu307, and His 448, and forms H-bonds with His447 (2.62 Å) and W1 (3.09 Å). The O2 atom of L-arabitol coordinates with Mn^{2+}, Glu307, Glu332, and His349, and forms H-bonds with W2 (3.14 Å). These coordinations are likely to help to fix the substrate in the proper conformation for the hydride or proton shift between the C1 and C2 of the substrate [36]. W1 and W2 are likely key water molecules responsible for the hydride or proton shift in the proposed catalytic mechanism, because they form H-bonds with the O1 and O2 atoms of L-arabitol, respectively. In addition, the O3 atom of L-arabitol H-bonds with His129 of the neighboring subunit (M2), and W3 forms multiple H-bonds with O4 atom of L-

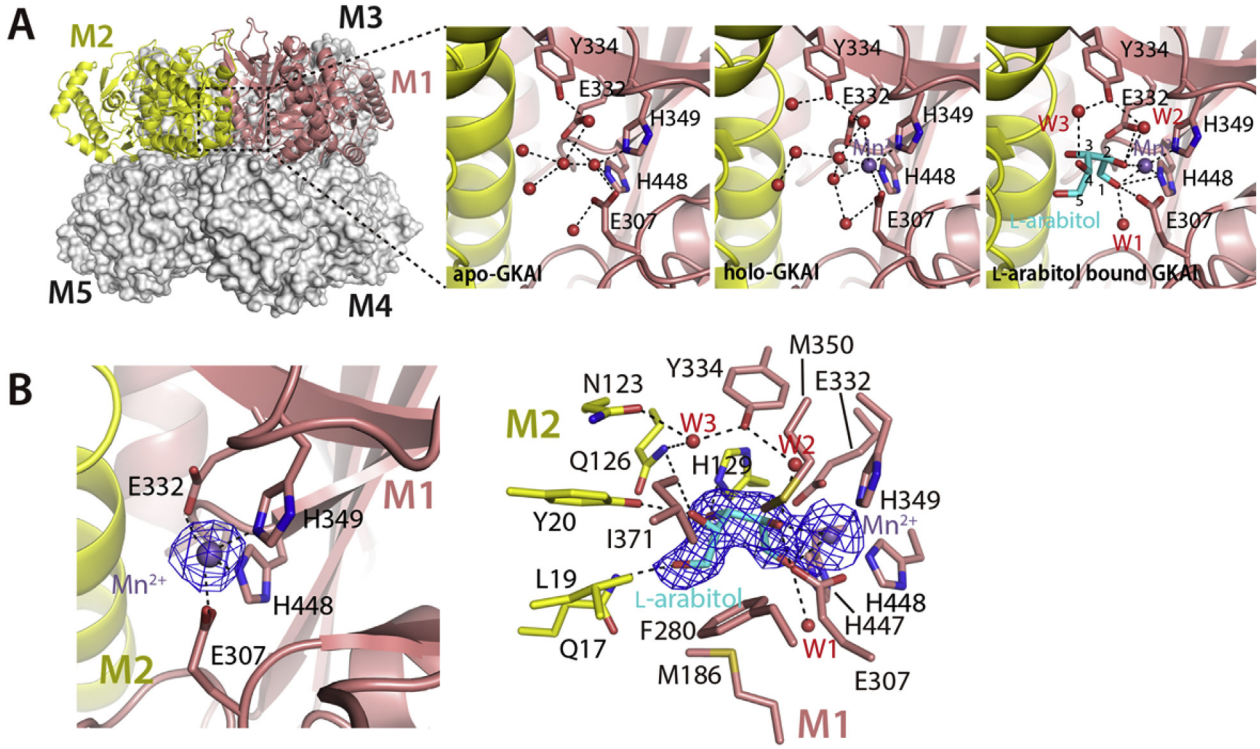

Fig. 3. Metal-binding and substrate-binding sites of GKAI. (A) The substrate binding site of GKAI at interface between two subunits are depicted as dotted rectangle box. Each of the monomers (M1 and M2) are colored in salmon and yellow, respectively. For simplification, other subunits are shown as surface structure in gray. Close-up view of the water-mediated H-bonds in the active sites of apo-, holo-, and L-arabitol bound GKAIs. Residues interacting with metal are depicted as sticks and the bound L-arabitol is shown in cyan stick. Mn^{2+} and water molecules are shown as slate and red spheres, respectively. H-bonds are shown as dashed line in black. Ligands and side chains are colored by atom type (oxygen in red and nitrogen in blue, respectively). (B) The mF_o-DF_c electron density map of Mn^{2+} (left panel) and L-arabitol (right panel) contoured at 2σ and represented to blue color. H-bonds are shown as dashed line. Residues interacting with metal and L-arabitol in GKAI are depicted as sticks. Mn^{2+} and water molecules are shown as purple and red spheres, respectively. The bound L-arabitol is shown in cyan stick. L-Arabitol in the active site of GKAI interacts with residues from M1 (salmon) and M2 (yellow) subunits and water molecules. Ligands and side chains are colored by atom type (oxygen in red, nitrogen in blue, and phosphorous in orange, respectively). (For interpretation of the references to colour in this figure legend, the reader is referred to the web version of this article.)

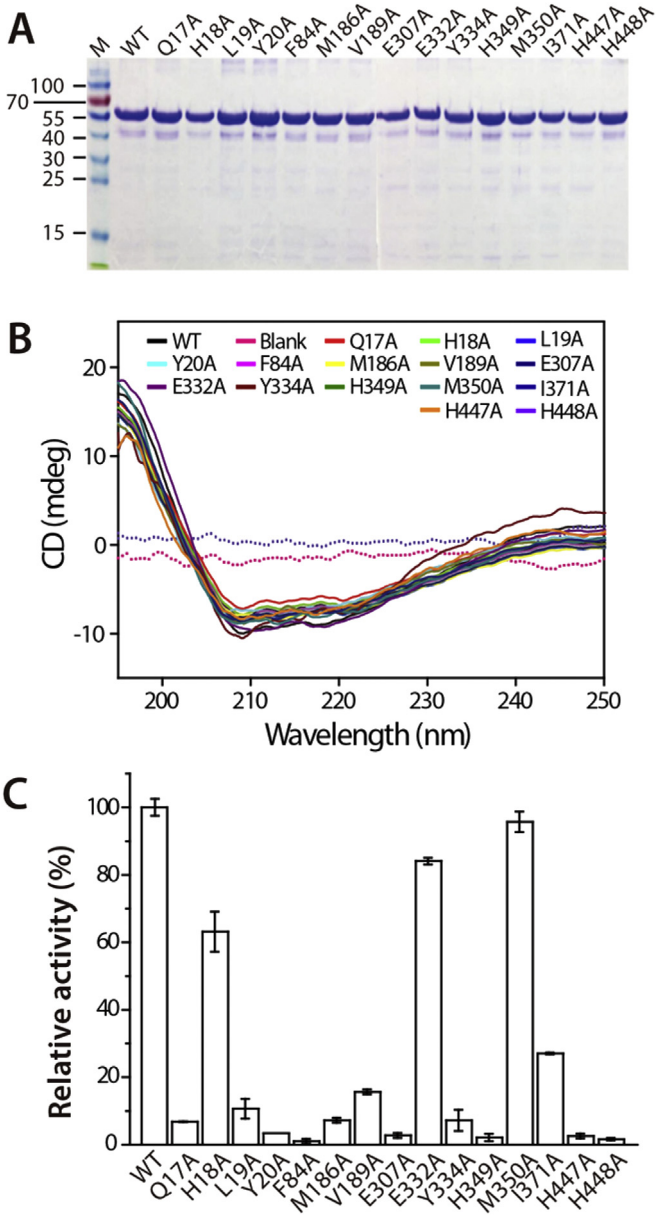

Fig. 4. The influence of mutations on the structural integrity and activity of GKAI. (A) SDS–PAGE of purified GKAI (WT) and its single mutants. (B) The CD spectra of the wild-type and single mutant AIs. (C) The effects of single mutations on AI activity. The AI activity of the wild-type enzyme for L-arabinose as a substrate was taken as 100%.

arabitol, Tyr334 (M1), Asn123 (M2), and Gln126 (M2) (Fig. 3A). Met186 and Met350 are coordinated by the O5 and O4 atoms, respectively, recognizing the hydroxyl groups at the 4 and 5 positions of L-arabitol, and C4 exhibits hydrophobic interactions with Phe280 (M1), Ile371 (M1), and Leu19 (M2) (Fig. 3B). Remarkably, O4 and O5 also form H-bonds with Tyr20 (M2, 2.56 Å) and Gln17 (M2, 2.93 Å), respectively, strongly indicating that the substrate-binding coordination occurs through intersubunit interactions.

The crystal structures of GKAI and its complex with L-arabitol as a substrate analogue showed that the enzyme undergoes large displacements of several amino acids, reflecting conformational changes in the course of catalysis. Remarkably, structural differences between the apo and holo forms of GKAI are observed in the recognition of atoms at the 4 and 5 positions of L-arabitol. Based on the observation that the structure of holo-GKAI was highly superimposed on that of L-arabitol bound GKAI in the presence of Mn^{2+},

Table 2
Kinetic parameters for GKAI (wild-type) and its single mutant AIs at 60 °C.

Enzyme	K_m (mM)	V_{max} (U/mg)	k_{cat}[b] (min^{-1})	k_{cat}[b]/k_m (mM^{-1} min^{-1})
Wild-type	11.3 ± 1.4[a]	19.8 ± 0.4	1113.5	81.9
Q17A	10.7 ± 0.9	4.7 ± 0.1	264.3	24.7
H18A	13.2 ± 0.4	7.3 ± 0.5	410.5	31.1
L19A	35.4 ± 8.7	1.9 ± 0.4	106.8	3.0
Y20A	NA[c]	NA	NA	NA
F84A	13.8 ± 6.8	1.0 ± 0.3	56.2	4.1
M186A	4.4 ± 0.5	2.8 ± 0.2	157.5	35.8
V189A	21.8 ± 4.8	3.7 ± 0.1	208.1	9.5
E307A	NA	NA	NA	NA
E332A	23.1 ± 1.0	12.5 ± 0.5	703.0	30.4
Y334A	9.9 ± 5.2	2.8 ± 0.1	157.5	15.9
H349A	NA	NA	NA	NA
M350A	8.4 ± 0.2	7.8 ± 0.1	438.6	52.2
I371A	16.6 ± 0.1	7.2 ± 0.1	404.9	24.4
H447A	NA	NA	NA	NA
H448A	NA	NA	NA	NA

[a] Data are means ± standard deviation.
[b] The k_{cat} is the number of substrate molecules reacted per active per min.
[c] NA, no activity.

holo-GKAI with L-arabitol can recognize substrates with different configurations of C4, C5, O4, and O5 by using Tyr20, Leu19 and Gln17, and *vice versa* (Figs. 5 and 3B). For example, O4 H-bonds with Tyr20, and C5 is coordinated with Leu19. In addition, Tyr20 and Leu19 of holo-GKAI are proximal to O4 of L-arabitol, respectively (Fig. 3B). By contrast, when the structure of L-arabitol -Mn^{2+}-GKAI was superimposed on that of apo-GKAI without L-arabitol, the corresponding Leu19 and Tyr20 residues of apo-GKAI were located 8.95 Å and 5.29 Å away from O4 atoms of L-arabitol, respectively (Fig. 5). Thus, the substrate recognition at the 4 and 5 positions of L-arabitol is thought to be less favorable for apo-GKAI than that of L-arabitol for holo-GKAI, a finding consistent with the significant lower enzyme activity of apo enzyme than that of the holo enzyme (Fig. 1). In addition, CD data demonstrated that site-directed mutagenesis on the substrate binding residues above did not lead to any significant perturbation of the structural integrity of each single mutant AI. Nevertheless, these mutant AIs exhibited less activity and/or lower catalytic efficiencies than the wild-type enzyme, which was probably due to lacking of any conformational changes in substrate binding (Table 2 and Fig. 4C). Therefore, substrate binding by GKAI involves the residues Met186 (β6–α7 loop), Met350 (β11–α14 loop), Ile371 (β12- β13 loop), and His447 (α15–β17 loop) of the M1 subunit, and Gln17 (M2), Leu19 (M2), and Tyr20 (β1–α1 loop, M2), in the N-terminal domain of the neighboring subunit.

3.5. Effect of metal ions on the structural stability of hexameric GKAI

To investigate the effect of metal ions on the structural stability of GKAI, we determined the oligomeric state of the apo and holo forms of GKAI using size-exclusion chromatography. As shown in Fig. 6A, as-isolated GKAI showed predominantly a hexameric structure, whereas apo-GKAI showed two distinct populations such as an intact hexamer and a partially unfolded and/or dissociated form. Remarkably, the addition of Mn^{2+} to apo-GKAI shifted significantly the oligomerization equilibrium toward an intact hexamer (α_6) as a major population, indicating that metal ions play an important role in the oligomerization of GKAI.

To further assess the effect of metal ions on the structural stability of the apo and holo forms of GKAI, we used differential scanning calorimetry (DSC) to determine their melting temperatures (T_m) (Fig. 6B). Intriguingly, thermal denaturation of apo-GKAI

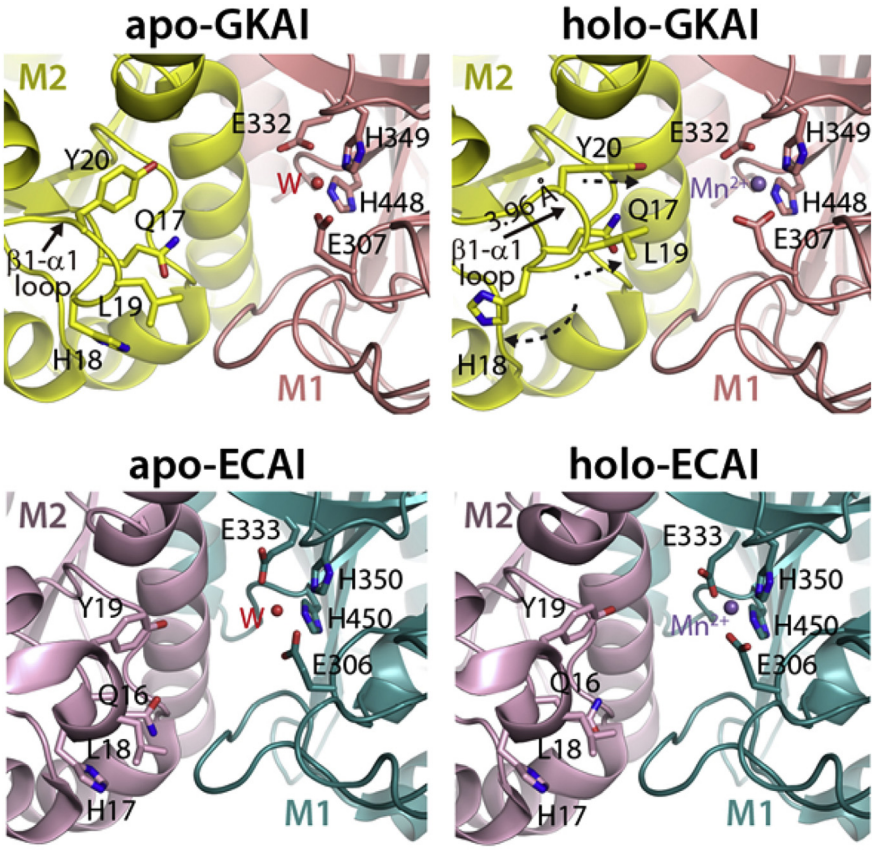

Fig. 5. Conformational change of the β1−α1 loop involved in the active site of GKAI and ECAI upon Mn^{2+}-binding. Compared with apo-GKAI, the β1−α1 loop of M2 subunit in holo-GKAI moves toward M1 subunit upon Mn^{2+}-binding. Displacement of residues on the β1−α1 loop is shown as dashed arrows in black. Side chains of M1 subunit (salmon) and M2 (yellow) residues that are involved in ligand coordination are represented as sticks. In contrast, such a conformational change is not observed in the corresponding β1−α1 loop regions of apo-ECAI (2AJT) and holo-ECAI (2HXJ). Ligands and side chains are colored by atom type (oxygen in red and nitrogen in blue, respectively). (For interpretation of the references to colour in this figure legend, the reader is referred to the web version of this article.)

revealed a major midpoint of thermal transition ($T_m = 71.09 \pm 0.56$ °C) with a minor one at 65.17 ± 1.44 °C, whereas holo-GKAI exhibited two thermal transitions at 78.94 ± 0.11 °C and 71.88 ± 0.34, respectively. Notably, the major and minor transition temperatures of holo-GKAI coincided with the T_m values of As-isolated GKAI, which were higher than the T_m values of apo-GKAI (Fig. 6B). Together with gel-filtration analysis, the DSC data thus clearly indicate that the holo form of GKAI is more thermodynamically stable than its apo form, suggesting that the binding of metal ions significantly contribute to the thermal stability of multimeric GKAI.

3.6. Structural basis for inter-subunit interactions

A hexameric structure consists of two identical trimers (i.e., upper and lower sides) stacked through head-to-tail contacts between monomers (Fig. 7). The PDBePISA calculations revealed that buried surface (total surface) areas of hexameric apo-, holo-, and L-arabitol-bound GKAI were 39,340 (89,030) Å^2, 40,120 (89,520) Å^2, and 46,230 (89,070) Å^2, respectively. Every subunit has three regions interacting with two adjacent monomers on the same side and one from the other side, with most of these reactions occurring through H-bonds and salt bridges (Fig. 7 and Table S1). Residues in the C-terminal domain of each subunit are in contact with those of the N-terminal domain of the neighboring subunit on the same side. In addition to these head-to-tail interactions on the same side, each subunit of a trimer was in contact with two monomeric subunits in the other trimer. Since two plates (a trimer per plate) are twisted around each other by 30°, α7 in the central domain of one subunit and the loop structure between β6 and α7 interact with the dimeric junction region formed by two domains of the other subunits (i.e., the central domain in one subunit and the N-terminal domain in the other subunit) (Fig. 7, M2-M5 interface). Along with the contact area between the central domains, the same residues in the same loop face each other in the 3D arrangement, with nine H-bonds and five strong salt bridges (i.e., Arg181:Asp184, Asp184:Arg181, Lys196:Glu193, Asp214:His284, and His284:Asp214) (Fig. 7, M1-M5 interface and Table S1). Two short α-helices, 7 and 3, run antiparallel, contacting each other *via* a salt bridge between Gln200 and Lys88 (Fig. 7, M2-M5 interface). Another important feature of the hexameric formation was that two α-helices (α2s) between the N-terminal domains of each subunit run antiparallel to each other by the salt bridges (Arg62:-Glu72 and Arg98:Glu96) and there are H-bondings among Arg62, Asn69, and Glu72 (Fig. 7, M2-M5 interface and Table S1). Additional contacts could also be deduced from active site, with salt bridges formed between Lys88:Asn208 and Asp195:Arg140.

CASTP (http://cast.engr.uic.edu) analysis revealed that the contact between the C-terminal domain of one subunit and the N-terminal domain of another subunit in apo-GKAI (M1-M2) created a major cavity for substrate binding (483.3 Å^3). The solvent accessible area (SAS) of the surface of the cavity (386.9 Å^2) is about 17% of the total SAS (2285 Å^2) (Table S3). This space is surrounded by the loop structures between β-strands 11 and 12 of the central and C-terminal domains in a subunit and the contact regions between the β-strand (β10) of the C-terminal domain and the α-helix (α4) and α4−α5 loop of the N-terminal domain in a neighboring unit (Fig. 7, M2-M1

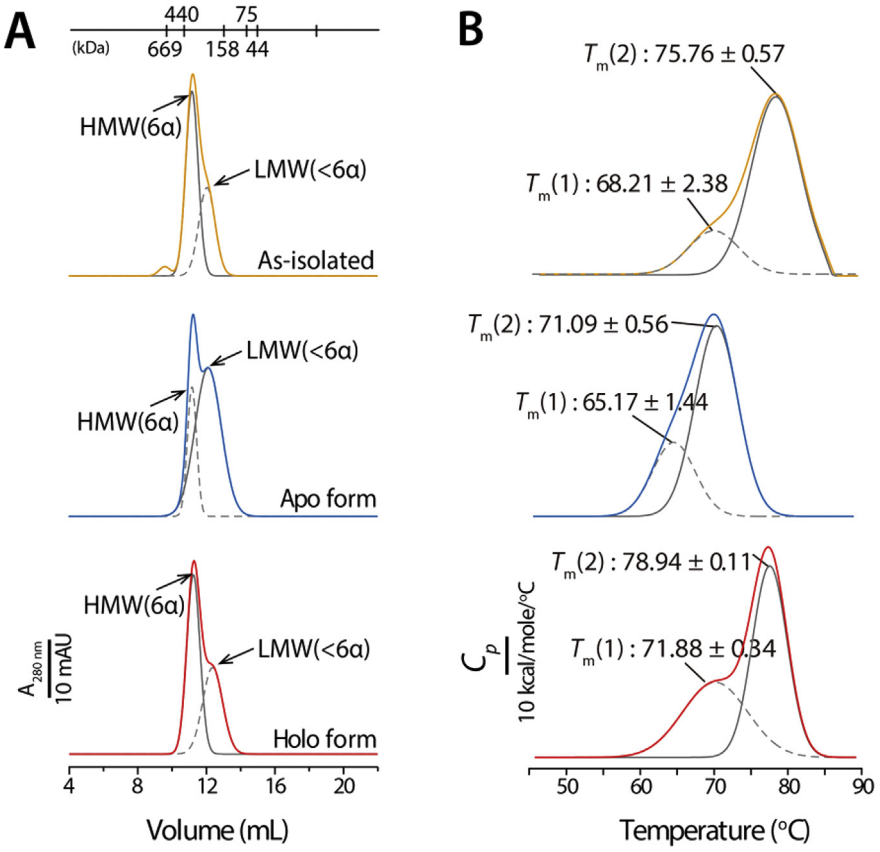

Fig. 6. (A) Size-exclusion chromatography for the apo and holo forms of GKAI. The Superdex 200 10/300 column (GE healthcare) was calibrated with protein size standards. HMW, high molecular weight; LMW, low molecular weight. (B) DSC data for the apo (blue line) and holo (red line) forms of GKAI. (For interpretation of the references to colour in this figure legend, the reader is referred to the web version of this article.)

interface). Other subunits with neighboring subunits (e.g., M2-M3 and M3-M1) were also arranged in the same manner. Consequently, the cavity can be divided into two distinct regions. One region forms an active site, with most residues on the loops from two subunits coordinating with metal and ligand, whereas the other region, extending from the active site, shows several direct interactions between β-strands (part of the β-barrel) of the C-terminal domain and the α-helix of the N-terminal domain of each subunit (Fig. 7 and Table S1). This space was formed by a combination of a β-barrel and α15 in the C-terminal domain and α5 from the N-terminal domain. Two important modes of inter-chain interactions are present inside the region. The penetration of a long side chain of Arg132 in α5 of the N-terminal domain allowed it to form a salt bridge and an H-bond with Asp333 (in β10) and Tyr336 in the C-terminal domain of a neighboring monomer, respectively (Fig. 7, M2-M1 interface). Although away from the region, His105 in β4 projecting into space is H-bonded to Tyr336. In addition, Arg132 links two H-bonds formed between His129 in α5 and Asp333, which creates serial interactions of two partitions in the region. These "serial alternative or staggered chain interactions" seem to tighten two adjacent subunits, providing the active site architecture surrounded by loops. In addition, the M2-M1 intersubunit interactions may be further stabilized by an additional H-bond between Arg145 in the M2 subunit and the carbonyl oxygen of Leu442 in the M1 subunit.

4. Discussion

Although (hyper)thermophilic AIs are quite advantageous for the commercial production of D-tagatose from D-galactose [13–18], their substrate specificities and thermostabilities, which are directly correlated with conversion efficiency, need to be further improved through protein engineering for a cost-effective biological process. Closer scrutiny of our crystal structures reveals the general principles of the novel structural AI fold and the molecular mechanism underlying metal-mediated catalysis and thermostability *via* intersubunit interactions. During aldose-ketose isomerization, one hydrogen is transferred as a proton between the electronegative oxygens of the hydroxyl and carbonyl groups of the aldose, whereas transfer of the second hydrogen from C-2 to C-1 may occur directly as a hydride (Fig. S1). Both isomerization can occur under aqueous conditions, with Mn^{2+} stabilizing the transition state for both reactions, suggesting that metal ion catalysis of isomerization provides a simple explanation for the requirement by GKAI of divalent metal ions [36]. The enzyme activity of thermostable AIs was highly dependent on metal ions for catalysis [7]. Moreover, in contrast to mesophilic AI, thermophilic AI undergoes conformational changes induced by Mn^{2+} at elevated temperatures [20]. Indeed, the crystal structures of the apo and holo forms of GKAI with and without bound L-arabitol elucidate the metal-dependent catalysis of AIs. Each monomer of hexameric GKAI undergoes large displacements of several amino acids upon metal and substrate binding (Fig. 5), supporting previous findings that the binding of Mn^{2+} to GKAI converts the inactive form of the enzyme into an active form at elevated temperatures. We thus conclude that GKAI may exhibit sequential, ordered kinetics, with Mn^{2+} binding first, followed by L-arabinose.

Despite the structural similarity of GKAI and ECAI, catalysis resistant to thermal inactivation is an intriguing issue. As described above, divalent metal ions significantly contributed to the overall architecture of GKAI (Fig. 6B), strongly indicating that metal-

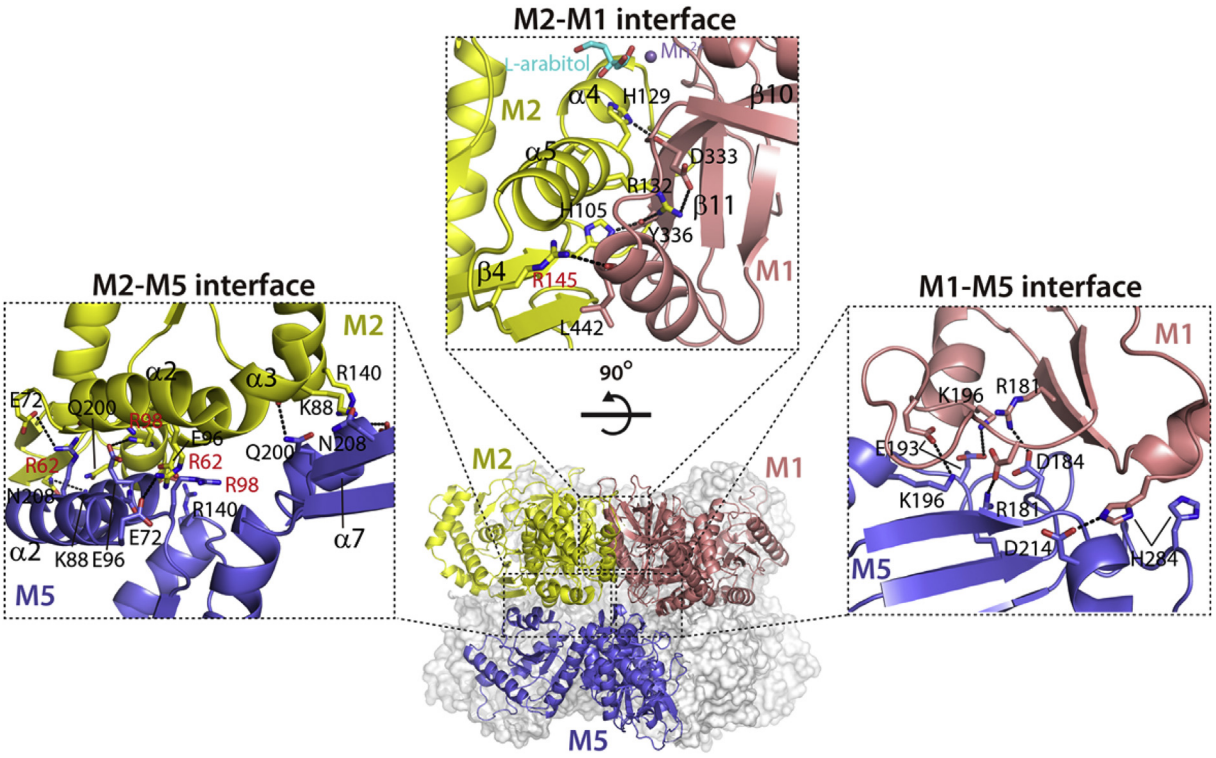

Fig. 7. Cavity formation of hexameric GKAI *via* intersubunit interactions. Interfaces between upper two subunits (M1 and M2) and lower one (M5) subunit are shown as rectangle dotted boxes. In M2-M5 interface, each monomer contacts in an antiparallel fashion, and forms salt bridges and H-bonds between α2–α2 and α3 (α7)–α7 (α3) helices, respectively (left panel). M1 and M5 subunits are in contact with each subunit through identical loop faces' interaction (right panel). Extended region for intersubunit interactions by residues of M1 and M2 subunits is shown as dashed lines (upper panel). The M1, M2 and M5 subunits are depicted as ribbon representations, and colored in salmon, yellow, and slate, respectively. Non-conserved Arg residues in GKAI are shown as red colored number. H-bonds and salt bridges are shown as dashed lines in black. (For interpretation of the references to colour in this figure legend, the reader is referred to the web version of this article.)

mediated transition of GKAI from the partially unfolded and/or dissociated form to an intact hexameric form is quite prerequisite not only for catalysis but also for the maintenance of oligomeric states of GKAI at elevated temperatures. Many studies have suggested that several factors are mainly involved in the thermostability of (hyper)thermophilic enzymes: for example, amino acid composition and changed environment of the active site surface [37,38]. These factors are highly associated with the proportion of charged residues (especially Arg) on interfaces and water-mediated H-bonds at the active site of an enzyme. For example, the Arg content of GKAI, >2%, is higher than that of other mesophilic sugar isomerizing enzymes, such as ECAI and ECFI (Table S2). Indeed, non-conserved Arg62 and Arg98 in the N-terminal domain of one subunit were found to be in contact with Glu72 and Glu96 in the N-terminal domain of another subunit, perhaps contributing to subunit interactions through four salt bridges since two trimeric units are in inverse contact, a contact not observed in mesophilic AIs (Fig. 7, M2-M5 interface). In addition, Arg145 was found to contribute to the H-bond with the peptide carbonyl oxygen of Leu442 (Fig. 7, M2-M1 interface). These results are consistent with previous findings, suggesting that more salt bridges/ion pairs (network of salt bridges) and H-bonds are key to increased thermostability [39,40]. Intriguingly, the breakdown of two intersubunit salt bridges was sufficient to have an adverse effect on the thermostability of hexameric thermostable glutamate dehydrogenases [41]. A single salt bridge rather than hydrophobic interaction can provide free energy of ~22 kJ/mol, contributing to the stabilization of protein folding at elevated temperatures, inasmuch as the stabilization of cellular proteins requires a free energy of ~50 kJ/mol [42,43]. In this regard, it was not surprising that GKAI was more stable than ECAI, inasmuch as the former had additional salt bridges, with more free energy of ~100 kJ/mol at 70 °C.

High resolution structures of GKAI also clearly showed the H-bonding networks at the active site in detail. Novel H-network formation by additional water-mediated H-bonds between amino acid residues and the substrate was found to stabilize the active site of a thermophilic xylanase during catalysis [44]. As shown in Fig. 3, the active site of apo-GKAI shows 2–3 more water-mediated H-bonds than that of apo-ECAI (2AJT), suggesting that thermophilic AI may tighten substrate binding with more H-bonding networks. Thus additional H-bonds found in the GKAI bound to L-arabitol may provide supportive evidence, that those water molecules play a major role in maintaining the integrity of the active site of the enzyme at elevated temperatures. Although several residues, including Leu19 and Tyr20 (Leu16 and Tyr17 in ECAI), are conserved, only the side chains in GKAI underwent significant conformational changes, resulting in its interaction with the substrate *via* H-bonds with water molecules. Moreover, we observed new water-mediated H-bonds to previously unknown substrates. Since individual H-bonds have an average free energy of 5.5 kJ/mol (~1.3 kcal/mol), contributing to enzyme stabilization [45], energy greater than ~20 kJ/mol may better stabilize the transition state of substrate in GKAI than in a mesophilic AI during catalysis. Although further investigations are needed, with additional structural studies on thermophilic enzymes, our findings provide a valuable example of the thermal stabilization of substrate mediated by substantial H-bonding, inasmuch as there were no such conformational changes in the corresponding residues in ECAI and ECFI. Therefore, we suggest that the extensive salt bridges in combination with H-bonds near the active sites may play important roles in supporting and maintaining the integrity of the catalytic site during functional assembly of hexameric AI monomers.

AIs have very low structural and sequence homology with other phosphosugar and non-phosphosugar isomerases, indicating that their structures are dissimilar, with no clear structure such as a general ketol isomerase fold. Therefore, the lack of both structural and sequence conservation suggests that AI is generally unrelated to these sugar isomerases. However, the apparent conservation of the overall fold in GKAI and ECFI crystal structures, despite their low sequence similarity, suggests that the overall fold may be conserved among AIs, with the overall fold therefore called an AI fold. Fig. 8 shows the superimposed substrate-binding structures of GKAI with bound L-arabitol, ECAI with bound D-ribitol (4F2D), and ECFI with bound inhibitor L-fucitol. The amino acid residues involved in metal binding are conserved, and the interactions of O1, O2 and O3 of L-arabitol in GKAI are very similar to those in ECAI, suggesting that the catalytic mechanism of metal-mediated proton transfer proposed for ECAI [46] also occurs for GKAI. In addition, the interactions between O1, O2, and O3 of L-fucitol and ECFI with Mn^{2+} are also quite similar to those of GKAI. In ECFI forming a crystallographic hexamer [27], the substrate-binding site for a neighboring molecule consists partly of the β1−α1 loop, and an extensively opened accessible surface is formed between M1 and M2, as found in GKAI (Fig. 8). In ECAI, however, the corresponding β1−α1 loop covers the bound metal ions in the same subunit, with a clear boundary between M1 and M2 with a relatively small contact area of 977 $Å^2$. In addition, the β1−α1 loop is not proximal enough to cover the substrate-binding site of the neighboring subunit (Fig. 5). In ECAI with D-ribitol, the corresponding residue is Leu18 (Leu19 in GKAI), located 4.3 Å from C5 of D-ribitol (L-arabitol in GKAI), with a large space between Leu18 and the bound substrate. In addition, His18 of GKAI is partly involved in electrostatic interactions by changing its side-chain conformation following the binding of a substrate, resulting in favorable interactions with the substrate. Thus the unique side-chain conformation around the hydroxyl group of C5, formed by residues Gln17, Leu19, and Tyr20 from the β1−α1 loop of GKAI, recognizes L-arabitol as the most suitable substrate, leading to the high substrate specificity of GKAI. In the absence of Mn^{2+}, however, the substrate-binding site of GKAI loosely recognizes both L-arabitol and D-galactose as substrates. This is consistent with the enzymatic activity of ECAI being much lower for D-galactose than that of GKAI.

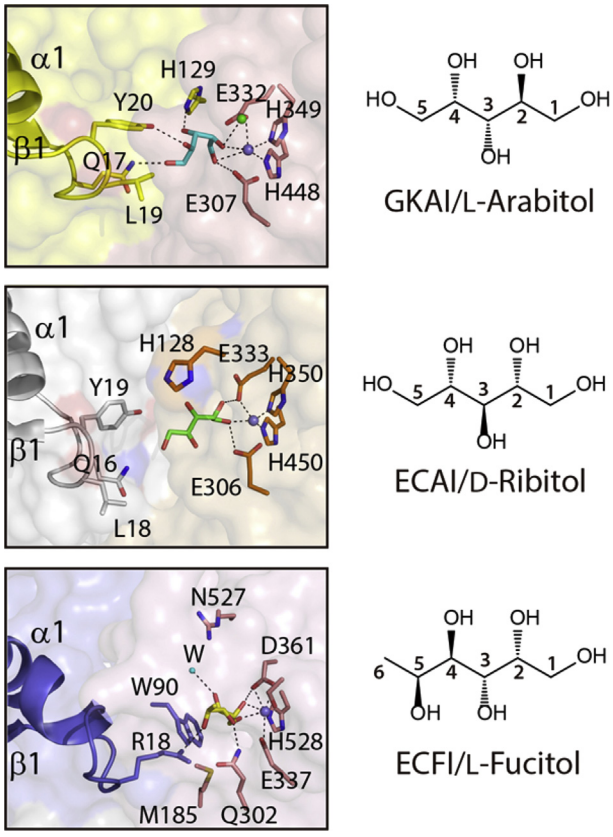

Fig. 8. Close-up view of the active sites of GKAI, ECAI, and ECFI. All three proteins are partly shown with a transparent surface and ribbon representation. Oxygen, nitrogen and sulfur residues are shown in red, blue and yellow, respectively. All residues shown are identical and/or corresponding to each other in GKAI, ECAI, and ECFI. Active site residues are shown as sticks in their subunit colors and are labeled. One subunit of GKAI and its neighboring subunit are depicted in yellow and whale, respectively. The substrate analogue L-arabitol is shown as cyon sticks. One subunit of ECAI and its neighboring subunit are depicted in white and orange, respectively. The inhibitor D-ribitol is shown as green sticks. One subunit of ECFI and its neighboring subunit are depicted in slate and pink, respectively. The substrate analogue L-fucitol is shown as yellow sticks. (For interpretation of the references to colour in this figure legend, the reader is referred to the web version of this article.)

Since L-arabinose and D-galactose have the same configurations of asymmetric carbon atoms as L-arabitol, their substrate-enzyme interactions are thought to be almost identical, but their enzyme activities are significantly different. The structural variation between L-arabitol and L-arabinose is found at the C5 position, where L-arabinose has a hydroxyl group instead of an aldehyde group and D-galactose has no group (Fig. 8). In the binding of D-galactose, a lack of hydrophobic interactions of C6 with the enzyme found in GKAI/L-arabitol may reduce enzyme activity toward D-galactose. Displacements of several amino acid residues restructure the substrate-binding site, so that D-galactose as the substrate is more accessible to mobilization. Because of the structural similarity of its substrates, which may be due to the sharing of hydroxyl groups at C3−C4 in a *cis*-configuration, AI can also catalyze the isomerization of D-galactose to D-tagatose [1,47].

5. Conclusion

In this study, we determined the functional and structural characteristics of a thermophilic L-arabinose isomerase (AI) that catalyzes the isomerization of L-arabinose (D-galactose) to L-ribulose (D-tagatose). Despite the fact that thermophilic AIs are used to produce an FDA-approved GRAS natural sweetener as well as a new antidiabetic and obesity control neutraceutical, little is known about the molecular basis underlying the substrate preferences and metal requirements of multimeric AIs because there has been no information about the structural and functional properties of these AIs up until now. We expressed and purified an AI from the thermophilic bacterium *G. kaustophilus*, and determined for the first time the crystal structures of its apo and holo forms as hexamers as well as that of holo-AI in complex with L-arabitol. The crystal structures not only provide a molecular basis for understanding the formation of the substrate-binding pockets through metal-mediated inter-subunit interactions, but also furnish a substrate-binding model for understanding isomerization reactions at elevated temperatures, which are distinct from those of its mesophilic counterparts.

Footnotes

This work was supported by the National Research Foundation of Korea (NRF) grants (2014R1A2A2A01006765 & 2013R1A1A2057465) to Dr. Dong-Woo Lee and to Dr. Sung Haeng Lee, respectively, funded by the Ministry of Science, ICT and Future Planning (MSIP), Korea, and by a Grant 311042-05-1-HD120 from the Korea Institute of Planning & Evaluation for Technology (iPET) funded by the Ministry for Food, Agriculture, Forestry and Fisheries to Dr. Dong-Woo Lee.

Acknowledgments

We thank the Beamline (PLS-5C) staff at the Pohang Light Source for technical support during data collection. We wish to confirm that there are no known conflicts of interest associated with this publication.

Appendix A. Supplementary data

Supplementary data related to this article can be found at http://dx.doi.org/10.1016/j.abb.2016.02.033.

References

[1] P.S.J. Cheetham, A.N. Wootton, Enzyme Microb. Technol. 15 (1993) 105–108.
[2] I. Sa-Nogueira, H. de Lencastre, J. Bacteriol. 171 (1989) 4088–4091.
[3] I. Sa-Nogueira, T.V. Nogueira, S. Soares, H. de Lencastre, Microbiology 143 (Pt. 3) (1997) 957–969.
[4] R. Schleif, Trends Genet. 16 (2000) 559–565.
[5] Y. Lu, G.V. Levin, T.W. Donner, Diabetes Obes. Metab. 10 (2008) 109–134.
[6] G.V. Levin, J. Med. Food 5 (2002) 23–36.
[7] D.W. Lee, H.J. Jang, E.A. Choe, B.C. Kim, S.J. Lee, S.B. Kim, Y.H. Hong, Y.R. Pyun, Appl. Environ. Microbiol. 70 (2004) 1397–1404.
[8] D.K. Oh, Appl. Microbiol. Biotechnol. 76 (2007) 1–8.
[9] P. Kim, Appl. Microbiol. Biotechnol. 65 (2004) 243–249.
[10] H.J. Roh, P. Kim, Y.C. Park, J.H. Choi, Biotechnol. Appl. Biochem. 31 (Pt. 1) (2000) 1–4.
[11] K. Yamanaka, Methods Enzymol. 41 (1975) 458–461.
[12] Y.B. Tewari, D.K. Steckler, R.N. Goldberg, Biophys. Chem. 22 (1985) 181–185.
[13] Y.H. Hong, D.W. Lee, S.J. Lee, E.A. Choe, S.B. Kim, Y.H. Lee, C.I. Cheigh, Y.R. Pyun, Biotechnol. Lett. 29 (2007) 569–574.
[14] F. Jorgensen, O.C. Hansen, P. Stougaard, Appl. Microbiol. Biotechnol. 64 (2004) 816–822.
[15] X.G. Hung, W.C. Tseng, S.M. Liu, W.S. Tzou, T.Y. Fang, Biochem. Eng. J. 83 (2014) 121–128.
[16] B.C. Lim, H.J. Kim, D.K. Oh, Appl. Biochem. Biotechnol. 149 (2008) 245–253.
[17] M. Rhimi, R. Ilhammami, G. Bajic, S. Boudebbouze, E. Maguin, R. Haser, N. Aghajari, Bioresour. Technol. 101 (2010) 9171–9177.
[18] M. Liang, M. Chen, X. Liu, Y. Zhai, X.W. Liu, H. Zhang, M. Xiao, P. Wang, Appl. Microbiol. Biotechnol. 93 (2012) 1469–1474.
[19] B.C. Kim, Y.H. Lee, H.S. Lee, D.W. Lee, E.A. Choe, Y.R. Pyun, FEMS Microbiol. Lett. 212 (2002) 121–126.
[20] D.W. Lee, E.A. Choe, S.B. Kim, S.H. Eom, Y.H. Hong, S.J. Lee, H.S. Lee, D.Y. Lee, Y.R. Pyun, Arch. Biochem. Biophys. 434 (2005) 333–343.
[21] D.W. Lee, Y.H. Hong, E.A. Choe, S.J. Lee, S.B. Kim, H.S. Lee, J.W. Oh, H.H. Shin, Y.R. Pyun, FEBS Lett. 579 (2005) 1261–1266.
[22] Y.H. Hong, D.W. Lee, Y.R. Pyun, S.H. Lee, J. Agric. Food Chem. 59 (2011) 12939–12947.
[23] S.J. Lee, Y.J. Lee, S.B. Kim, S.K. Kim, D.W. Lee, Appl. Environ. Microbiol. 78 (2012) 8813–8816.
[24] J.W. Patrick, N. Lee, J. Biol. Chem. 243 (1968) 4312–4318.
[25] J.W. Patrick, N. Lee, J. Biol. Chem. 244 (1969) 4277–4283.
[26] B.A. Manjasetty, M.R. Chance, J. Mol. Biol. 360 (2006) 297–309.
[27] J.E. Seemann, G.E. Schulz, J. Mol. Biol. 273 (1997) 256–268.
[28] Y.J. Lee, S.J. Lee, S.B. Kim, S.H. Lee, D.W. Lee, FEBS Lett. 588 (2014) 1064–1070.
[29] T.N. Nazina, T.P. Tourova, A.B. Poltaraus, E.V. Novikova, A.A. Grigoryan, A.E. Ivanova, A.M. Lysenko, V.V. Petrunyaka, G.A. Osipov, S.S. Belyaev, M.V. Ivanov, Int. J. Syst. Evol. Microbiol. 51 (2001) 433–446.
[30] H. Takami, Y. Takaki, G.J. Chee, S. Nishi, S. Shimamura, H. Suzuki, S. Matsui, I. Uchiyama, Nucleic Acids Res. 32 (2004) 6292–6303.
[31] D.W. Lee, D. Kim, Y.J. Lee, J.A. Kim, J.Y. Choi, S. Kang, J.G. Pan, Proteomics 13 (2013) 2278–2282.
[32] T.P. Cao, J.M. Choi, S.J. Lee, Y.J. Lee, S.K. Lee, Y. Jun, D.W. Lee, S.H. Lee, Acta Crystallogr. F. Struct. Biol. Commun. 70 (2014) 108–112.
[33] Z. Dische, E. Borenfreund, J. Biol. Chem. 192 (1951) 583–587.
[34] P.D. Adams, R.W. Grosse-Kunstleve, L.W. Hung, T.R. Ioerger, A.J. McCoy, N.W. Moriarty, R.J. Read, J.C. Sacchettini, N.K. Sauter, T.C. Terwilliger, Acta Crystallogr. D. Biol. Crystallogr. 58 (2002) 1948–1954.
[35] S. Dietmann, J. Park, C. Notredame, A. Heger, M. Lappe, L. Holm, Nucleic Acids Res. 29 (2001) 55–57.
[36] R.W. Nagorski, J.P. Richard, J. Am. Chem. Soc. 123 (2001) 794–802.
[37] C. Vieille, G.J. Zeikus, Microbiol. Mol. Biol. Rev. 65 (2001) 1–43.
[38] T.J. Taylor, I.I. Vaisman, BMC Struct. Biol. 10 (Suppl. 1) (2010) S5.
[39] D. Maes, J.P. Zeelen, N. Thanki, N. Beaucamp, M. Alvarez, M.H. Thi, J. Backmann, J.A. Martial, L. Wyns, R. Jaenicke, R.K. Wierenga, Proteins 37 (1999) 441–453.
[40] S. Kumar, C.J. Tsai, R. Nussinov, Protein Eng. 13 (2000) 179–191.
[41] C. Vetriani, D.L. Maeder, N. Tolliday, K.S. Yip, T.J. Stillman, K.L. Britton, D.W. Rice, H.H. Klump, F.T. Robb, Proc. Natl. Acad. Sci. U. S. A. 95 (1998) 12300–12305.
[42] R. Jaenicke, FEMS Microbiol. Rev. 18 (1996) 215–224.
[43] P.L. Privalov, S.J. Gill, Adv. Protein Chem. 39 (1988) 191–234.
[44] A.L. van Bueren, S. Otani, E.P. Friis, K.S. Wilson, G.J. Davies, Acta Crystallogr. Sect. F. Struct. Biol. Cryst. Commun. 68 (2012) 141–144.
[45] B.A. Shirley, P. Stanssens, U. Hahn, C.N. Pace, Biochemistry 31 (1992) 725–732.
[46] S. Banerjee, F. Anderson, G.K. Farber, Protein Eng. 8 (1995) 1189–1195.
[47] K. Izumori, Y. Ueda, K. Yamanaka, J. Bacteriol. 133 (1978) 413–414.